Available online at www.sciencedirect.com

ScienceDirect

Journal of the Franklin Institute 356 (2019) 2505–2529

www.elsevier.com/locate/jfranklin

Education Article

Robust multivariable predictive control for laser-aided powder deposition processes

Xiaoqing Cao*, Beshah Ayalew

Applied Dynamics and Control Group, Clemson University-International Center for Automotive Research, Greenville, SC 29607, USA

Received 30 April 2018; received in revised form 15 October 2018; accepted 10 December 2018
Available online 10 February 2019

Abstract

This paper presents a robust multivariable predictive control for laser-aided powder deposition (LAPD) processes in additive manufacturing. First, a novel control-oriented *MIMO* process model is derived. Then, the objective of achieving desired geometrical and thermal properties is formulated as one of generating and tracking nominal reference profiles of layer height and melting pool temperature. This is accomplished via a nonlinear model predictive control with guaranteed nominal stability. Furthermore, a local ancillary feedback law is derived to provide robustness to bounded uncertainties. The paper verifies the effectiveness of the proposed control via a case study on a laser cladding process.

1. Introduction

LASER aided powder deposition (LAPD) encompasses a wide range of advanced additive manufacturing processes such as laser cladding, selective laser sintering (SLS), laser metal deposition (LMD), laser solid freeform fabrication (LSFF), etc. [1,2]. The essence of LAPD is that fully functional metal components can be fabricated directly from computer aided design (CAD) models via layer-by-layer material deposition. This enables the ability to manufacture industrial products with more complex geometries while reducing product weight, material wastage as well as production cycle time, compared with conventional “subtractive” manufacturing techniques [3,4].

* Corresponding author.
E-mail addresses: xiaoqin@g.clemson.edu (X. Cao), beshah@clemson.edu (B. Ayalew).

https://doi.org/10.1016/j.jfranklin.2018.12.015

Despite such promising prospects, there are still challenges for LAPD processes to achieve satisfactory product quality requirements [3]. Among the various requirements, the dimensional accuracy is perhaps one of the most important. This often includes deposited layer height and width, which determine the deposition profile, surface finish and homogeneity of layers and contributes to the uniformity and repeatability of the whole process [5]. As it is pointed out in [6], LAPD is a thermal-dominated process in which melting pool temperature is another important factor that has to be considered. It determines critical process properties such as powder catch efficiency, melting pool dimension, dilution and product defects such as porosity and cracking due to thermal stresses [5]. Moreover, the melting pool temperature may even reflect the height of deposition (degree of lack of deposition) as mentioned in [7]. More importantly, due to the complex interactions and the inherent multi-input-multi-output (*MIMO*) process characteristics, simultaneous monitoring and regulation of these two factors are often required. This motivates the need for a systematic control scheme design for LAPD processes.

To this end, suitable process models are needed. Detailed models for LAPD processes involve coupled nonlinear partial differential equations (PDEs) that describe the complex multi-physics involving heat transfer, fluid flow and laser-powder interactions [8–11]. However, from the perspective of control system design and implementation, these models are neither analytically nor computationally expedient. Lumped parameter models in the form of ordinary differential equations (ODEs) or their equivalent forms are preferred [6,7,12,13]. In this paper, a control-oriented process model suitable for control design is proposed that retains the inherent *MIMO* characteristics and nonlinear dynamical coupling between the main process variables. This is subsequently used for robust multivariable predictive control design.

In the literature, the commonly used control system designs for LAPD processes are proportional-integral-derivative (PID) controllers [12–15] and their extensions combined with feedforward scheme [6] or parameter adaption law [16]. These approaches largely sidestep the lack of formal process models. Recently, advanced control strategies such as the general predictive control [7], variable structure control [17] and iterative learning control [18] have been proposed for closed-loop regulation of similar processes. However, these control schemes were only shown to regulate a specific process output by adjusting a corresponding input in a single-input-single-output (SISO) manner. In [19], a two-input-single-output (MISO, with two inputs to the controller) hybrid control system that includes a master height controller and a slave temperature controller is designed to control both layer height and melting pool temperature in a direct metal deposition process. Although this expands the potential of controlling multiple process outputs simultaneously, a control system design via a single control variable, such as the laser power, has limited capabilities as pointed out in [13,19]. This recognition motivates the inclusion of another control variable, such as the laser scanning speed, to achieve effective process control under a *MIMO* framework, providing a wider range of operating conditions [13].

To design a proper *MIMO* control system for LAPD processes, following challenges need to be considered: (1) given the nonlinear coupling between layer height and melting pool temperature, simultaneous regulation of these two variables is highly desirable; (2) there are practical constraints on the individual control inputs and process variables, such as the maximum laser power, scanning speed or allowable pool temperature. These constraints inherent in the LAPD process have to be considered while devising the controllers. Given its well-known ability to deal with hard constraints in multivariable processes, model predictive control (MPC) is well suited for control system design of LAPD processes [19–21]. Since actual operating parameters/conditions may deviate from their nominal model predicted values due to potential disturbances (modeling uncertainty, parameter shift, exogenous disturbances, etc.), robust versions of MPC have to be considered. Theoretical designs of robust predictive control include the *min–max* open-loop MPC that considers the worst case objective [20,22], and also the H_∞-MPC that incorporates an auxiliary control derived from the H_∞ theory [23–25]. However, the computational complexity of these methods hinders their implementable control system designs for complex nonlinear processes such as LAPD. Based on the similar idea of constraint-tightening MPC [26,27], the *tube-based* MPC method is considered as an implementable control scheme which combines feedforward and state-feedback control [28,29]. The feedforward term is derived from the nominal MPC scheme and generates a nominal reference trajectory which serves as the central path of the tube [28]. The state-feedback control, which is also known as the ancillary control, is devised to act locally such that all the possible trajectories in the presence of uncertainties are steered close to the reference trajectory. Some reported applications of this method include the robust control of mobile robots [30,31] and semi-autonomous vehicles [32,33].

The purpose of this paper is to propose and demonstrate a systematic modeling and control scheme for a class of LAPD processes. The key contributions of our work are: (1) A control-oriented *MIMO* process model, which is capable of capturing the inherent nonlinear coupling (between deposited layer height and melting pool temperature) and facilitates multivariable control design for the process; (2) A nonlinear model predictive control (NMPC) scheme that generates the nominal trajectory based on product geometric and thermal specifications with guaranteed stability. (3) A tube-based ancillary control design based on local linear feedback, providing robustness to some unstructured uncertainties. Brief versions of the first two contributions were presented in our ACC papers [21,34]. They are also included in this paper to enhance the completeness of the whole control design. The robustness consideration and the tube-based MPC design for LAPD processes are new derivations presented in this paper. In addition, the case study results appear here for the first time. The overall proposed control method in this paper is aimed to fill the gap between the well-recognized needs for multivariable process control and the lack of formal *MIMO* models and therefore model-based control designs for LAPD processes [13,19].

The rest of the paper is organized as follows: Section 2 discusses the modeling of LAPD processes where the control-oriented *MIMO* process model is introduced. An offline parameter identification method is proposed to extract unknown process parameters before controller implementation. Section 3 details the design of tube-based multivariable predictive control method. This includes both the formulation of the nominal nonlinear predictive control and the design of the ancillary control. Section 4 provides a case study on the laser cladding process. Therein, the effectiveness of the proposed approach is demonstrated. Section 5 gives the conclusions of the work.

2. Modeling of LAPD processes

2.1. Process overview

LAPD systems generally consist of a high-intensity laser source with beam delivery optics, material supply system, motion system and process monitoring and control unit. The LAPD process set up we consider in this paper is illustrated in Fig. 1.

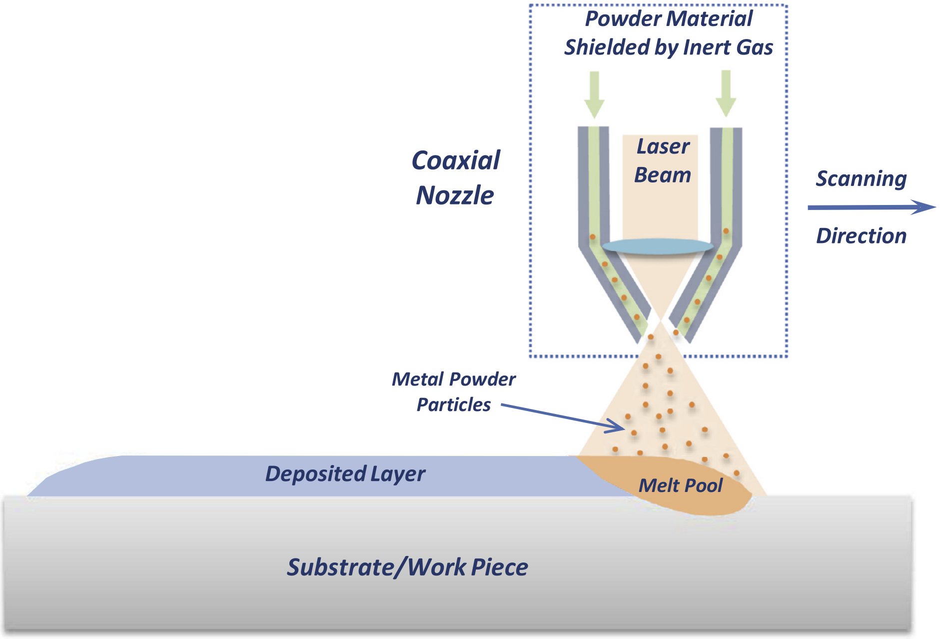

Fig. 1. Schematic of the LAPD processes.

The laser beam generated by the laser source is transported by beam delivery optics (e.g., optical fibers and lenses) to the top surface of the substrate, creating a melting pool. The powder materials are directed with carrier gas, such as nitrogen, into the melting pool area by the material supply system. With the relative movements created by the motion system (either robotic manipulators or CNC tables), the laser beam and powder material sweep on the substrate, forming depositions of a single layer or even build-up layers. Sensor suits such as high-speed CCD cameras or infrared cameras and pyrometers are often incorporated for in-process monitoring and closed-loop feedback control. For further details on the process setup, the reader is refer to [35,36].

2.2. *Control-oriented* MIMO *process modeling*

For effective control system design and implementation, lumped parameter models are desired. In order to derive such a model for LAPD processes, we make the following simplifying assumptions:

(1) The melting pool can be approximated by a semi-ellipse with length L, width W and height H as illustrated in Fig. 2 [16].
(2) The melting pool aspect ratio (width/length) is empirically related to laser power q and scanning speed v by empirical constants D, E as: $\frac{L}{W} = 1 + (Dq + E)v$ [37]. It is worth noting that these empirical constants are subject to process configurations (e.g., laser type/power, nozzle configuration, standoff distance, etc.) and so these parameters are to be determined by prior parameter identification (fitting) for the particular hardware configuration.

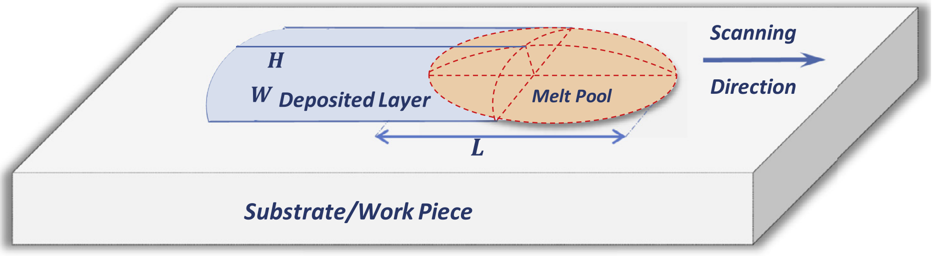

Fig. 2. Melting pool geometry approximated by semi-ellipse.

(3) The deposited track-width approximately remains constant and is determined by the laser beam diameter [38–40]. This constant track-width is denoted by W_0 in the rest of this paper.

The derivation of the *MIMO* lumped model is based on the mass and energy balance equations, along with modifications of temperature-dependent powder catch efficiency and input-dependent laser absorptivity. The mass balance in the melting pool can be expressed as [16]:

$$\rho_l \dot{V} = \eta_m \dot{m}_P - \rho_l A v \tag{1}$$

where $V = \frac{\pi}{6} W_0 H L$ is the total volume of the melting pool; $A = \frac{\pi}{4} W_0 H$ is the cross-sectional area in the transverse plane; $\eta_m \dot{m}_P$ denotes the amount of powder material that is deposited into the melting pool per unit time, where $\dot{m}_P$ is the powder feed rate from the nozzle. η_m is the powder catch efficiency (ratio of deposited powder to total injected powder), which is modeled as a function of melting pool temperature T:

$$\eta_m(T) = \begin{cases} \eta_{m0} * \left[1 - e^{-k_T(T - T_m)}\right], & T > T_m \\ 0, & T \le T_m \end{cases} \tag{2}$$

Remark 1. Close examination of the physical phenomena involved and experimental tests show that laser-aided powder deposition is a thermal-dominated process [6]. The melting pool temperature affects not only the material property but also the deposition height of the final products [5,7]. Moreover, due to the fact that the powder material can only be successfully deposited in the melting pool area (where $T > T_m$, T_m is the constant melting temperature for the specific material), melting pool temperature is selected as the main process parameter that determines the powder catch efficiency in Eq. (2). The parameter η_{m0} is the maximum powder catch efficiency. With the specific nozzle configuration (including laser beam distribution, powder distribution, etc.) both η_{m0} and k_T are assumed to be process constants. Identification of these parameters will be discussed further later.

With constant laser power and scanning speed, the melting pool moves at the same speed as the laser source and the pool geometry stays approximately the same in steady state [41]. Thus, the quasi-steady-state deposited layer height can be derived by equating the left term in the mass balance equation to zero:

$$H_{ss} = \frac{4 \eta_m \dot{m}_P}{\pi \rho_l W_0 v} \tag{3}$$

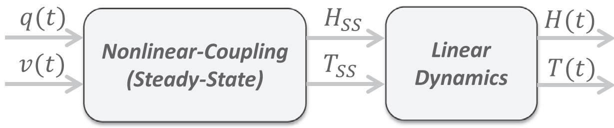

Fig. 3. Structure of the control-oriented *MIMO* LAPD process model.

The energy balance in the melting pool is given by [34]:

$$\rho_l \, (\dot{V\sigma}) = \eta_q q - A_s h_s (T - T_m) - A_g h_g (T - T_0) - \delta_{S/L} \tag{4}$$

In this equation, the left-hand side stands for the rate of energy change in the melting pool, whereas the right-hand side consists, respectively, of the total rate of energy input from the laser irradiation, the rate of energy loss due to convection on liquid/solid and liquid/gas interfaces and the rate of energy loss from the melting pool due to the effects of solidification and melting. σ is the specific internal energy and is defined as: $\sigma(T) = C_s(T_m - T_0) + \mathcal{L} + C_l(T - T_m)$, T_0 is the ambient temperature. C_s and C_l denote the solid and liquid heat capacity, respectively, whereas $\mathcal{L}$ is the latent heat of fusion. Both the heat capacity and latent heat of fusion are material-specific and are assumed to be known. The absorbed laser power in the melting pool can be modeled as $\eta_q q$, in which, η_q denotes the laser absorptivity and can be modeled as:

$$\eta_q(q, v) = \eta_{q0} * \left(1 - e^{-k_q q}\right) * e^{-k_v v} \tag{5}$$

Remark 2. This model is suggested from closely examining how the laser power q and scanning speed v affect the temperature distribution and the shape of melting pool on the substrate. Based on the geometric relationship between the melting pool shape and laser power distribution, laser irradiation area can be determined. η_{q0}, k_q, k_v are positive process constants to be identified with identification experiments described later.

The heat convection areas on liquid/solid and liquid/gas interfaces are given by: $A_s = \frac{\pi}{4} W_0 L$, $A_g = 2\pi * \left(\frac{\left(\frac{W_0}{2} * \frac{L}{2}\right)^{1.6} + \left(\frac{W_0}{2} * H\right)^{1.6} + \left(\frac{L}{2} * H\right)^{1.6}}{3}\right)^{1/1.6}$. h_s and h_g are the respective heat convection coefficients and they are assumed to be constant during the process. In steady state, the melting pool moves at the same speed as the laser source and the surface geometry remains approximately the same. Therefore, the solidification and melting speed can be assumed the same and the energy loss due to the effect of solidification and melting ($\delta_{S/L}$) vanishes. Thus, the steady-state temperature can be derived as:

$$T_{ss} = \frac{\eta_q q + A_s h_s T_m + A_g h_g T_0}{A_s h_s + A_g h_g} \tag{6}$$

As pointed out in [6], LAPD processes are dominated by thermal effects whose dynamics can be approximated with a first-order linear system. We concatenate this linear block with the expressions derived above that capture the nonlinear coupling in steady state. This is formally a Hammerstein type model as shown in Fig. 3.

In this model, the coupled dynamics of deposited layer height and melting pool temperature are approximated with a memoryless nonlinear function (steady-state relation) followed by a linear first-order block. The system dynamics equations are:

$$SYS_t : \begin{cases} \dot{H} = \frac{1}{\tau_H} * \left(\frac{4\eta_m \dot{m}_P}{\pi \rho_l W_0 v} - H \right) \\ \dot{T} = \frac{1}{\tau_T} * \left(\frac{\eta_q q + A_s h_s T_m + A_g h_g T_0}{A_s h_s + A_g h_g} - T \right) \end{cases} \tag{7}$$

where τ_H and τ_T are time constants.

Assumption 1. Note that in this *MIMO* model, both process states are assumed to be measureable. This can be achieved via appropriate sensors such as high-speed CCD cameras for deposited layer height sensing and radiation pyrometers for melting pool temperature measurement [3]. Due to the comparatively slow response of the powder delivery system, powder feed rate is not considered as a control variable here [13]. Moreover, process configuration parameters such as the nozzle standoff distance/orientation, laser beam radius, powder feed rate and distribution, are assumed to be fixed. This assumption arises from the persistent trade-off between model fidelity and computational efficiency in control system design. Modeling uncertainties resulting from potential variations in these parameters could be properly handled by the robust controller design to be discussed in Section 3.

2.3. Parameter identification

In this section, identification of unknown parameters in the process model is briefly introduced. This is usually conducted offline with the availability of process data. The parameters to be identified include: time constants τ_H, τ_T; empirical constants D, E in melting pool aspect ratio; powder catch efficiency parameters η_{m0}, k_T and laser absorptivity parameters η_{q0}, k_q and k_v. We use $\Theta = [\tau_H, \tau_T, D, E, \eta_{m0}, k_T, \eta_{q0},\ k_q,\ k_v]^T$ to denote the unknown parameter vector for brevity.

To obtain a set of process data for parameter identification, a finite element model (FEM) implemented in *COMSOL Multiphysics* is treated as the actual process for its explicit considerations of the multi-physics phenomena and their interactions in the process. The multi-physics model is detailed in our previous work [34]. By predefining a control input vector $\mho$ with variable laser power and scanning speed, the process output data, namely the deposited layer height H and average melting pool temperature T are obtained from simulations of the FEM. Then, the parameter identification task is formulated as a constrained optimization problem as follows:

$$Min_{\Theta}\ J(H, T, \mho) \tag{8}$$

$$Subject\ to:\ \ SYS_t(H, T, \mho)$$

where, the objective function J is defined as:

$$J = \int_t \left[\alpha_1 \left(H(\tau) - H_p \right)^2 + \alpha_2 \left(T(\tau) - T_p \right)^2 \right] d\tau \tag{9}$$

where α_1 and α_2 are positive weighting constants. Subscript p denotes the variables from the actual process (FEM). By defining this objective function, the errors between the process and proposed *MIMO* model outputs are quantified and then minimized by searching for an optimal set of the unknown parameters in vector Θ. This optimization is implemented in

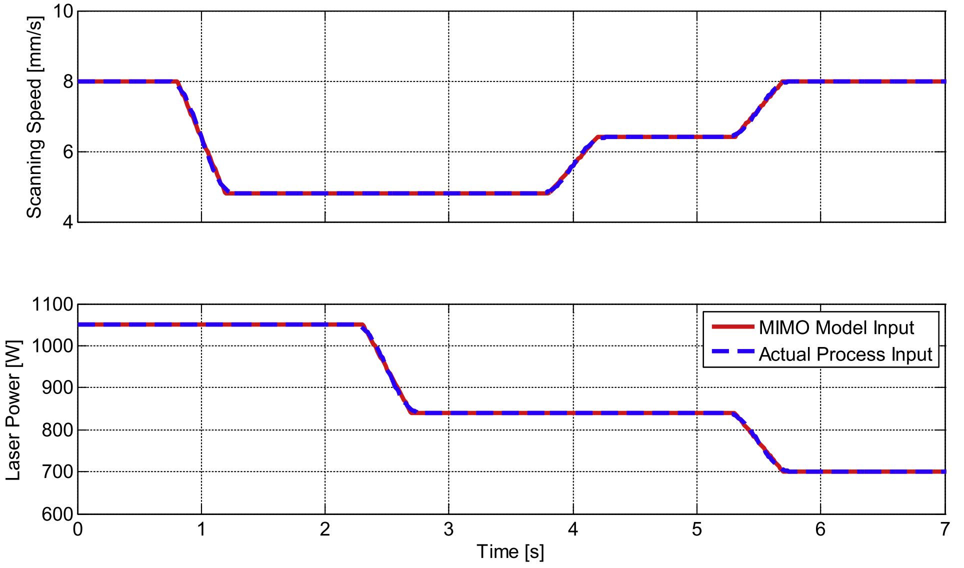

Fig. 4. Plant/model laser power and scanning speed.

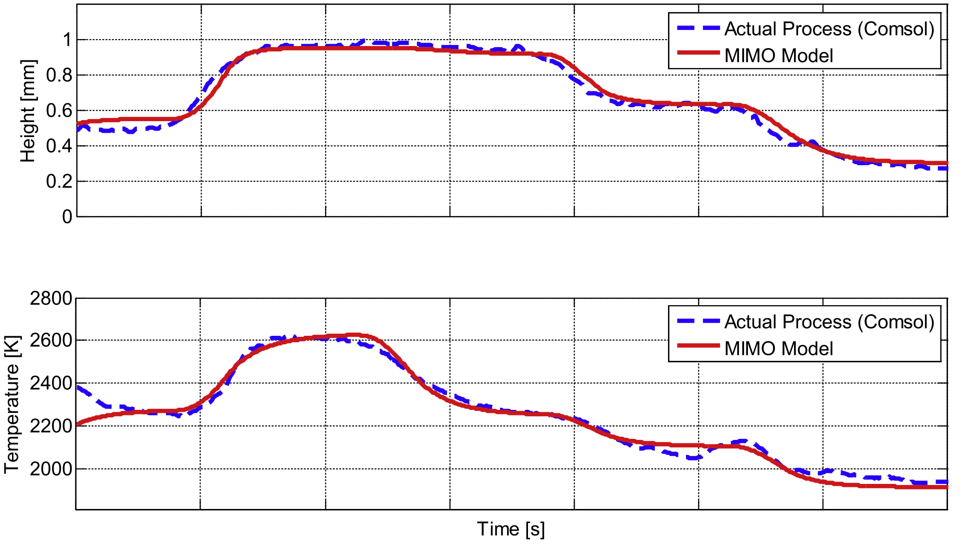

Fig. 5. Plant/model deposition height and melting pool temperature.

Matlab where the solution is obtained by the classical Nelder–Mead simplex method. The identified unknown parameters are listed in the following table.

The control input sequences and the comparison results of the parameter identification experiments are illustrated in Figs. 4 and 5 as follows:

Fig. 4 shows the open-loop input sequences, i.e., the combination of laser power and scanning speed used for parameter identification. They are assumed to be time-dependent step functions with sufficient smoothness for the finite element solver. The model/plant comparison

Table 1
Identified parameters in proposed model.

Parameter	Meaning	Value	Unit
$\boldsymbol{\tau_H}$	Time constant for height	0.1145	[s]
$\boldsymbol{\tau_T}$	Time constant for temperature	0.2898	[s]
$\boldsymbol{\eta_{m0}}$	Powder catch efficiency parameter	0.4224	[l]
$\boldsymbol{k_T}$	Powder catch efficiency parameter	0.0072	[1/K]
$\boldsymbol{\eta_{q0}}$	Laser absorptivity parameter	0.0545	[1]
$\boldsymbol{k_q}$	Laser absorptivity parameter	1.357×10^{-4}	[1/W]
$\boldsymbol{k_v}$	Laser absorptivity parameter	332.8	[s/m]
$\boldsymbol{D}$	Empirical constant	−0.0769	[s/m/W]
$\boldsymbol{E}$	Empirical constant	−0.9071	[s/m]

of deposited layer height and melting pool temperature is shown in Fig. 5. We can see that the layer height from the proposed *MIMO* model follows the value in the actual process fairly well over the whole simulated duration. The relative error (the root-mean-square-error with respect to the maximum values) of the layer height is 3.44%, which shows a relatively good agreement between the detailed process model (FEM) and the proposed model. The temperature output from the model shows some deviation from the actual plant (FEM) value at the beginning. This is possibly due to the complex phase change dynamics occurring during the initial development of the melting pool, which is not considered in the proposed lumped model. Despite this, the proposed model captures the actual temperature dynamics well, with only a 1.32% relative error. This identified model is also validated with other sets of input combinations. For more detailed discussion of this part, we refer the reader to our ACC paper [34].

With the identified process parameters shown in Table 1, an online multivariable predictive control can be formulated to achieve desired system performance. This is detailed in following section.

2.4. Control problem formulation

Before formulating the control problem, we introduce a transformation to use a spatial coordinate as the independent variable instead of time. In LAPD processes, the desired part geometry model is often designed in CAD software and this model is then sliced into different layers with pre-planned material deposition paths. In other words, during the deposition of each layer, the scanning route of the laser/nozzle is pre-defined in a fixed spatial domain (the deposition track length). Meanwhile, since the scanning speed is a manipulated control input, the process time domain is not necessarily fixed (e.g., leading to a variable process end-time). Thus, to facilitate the controller design, a coordinate transformation is needed to express the process model in a fixed spatial S-coordinate of the same direction as that of the laser scanning. Then,

$$\begin{cases} \dot{H} = \dfrac{dH}{ds}\dfrac{ds}{dt} = \dfrac{dH}{ds}v \\ \dot{T} = \dfrac{dT}{ds}\dfrac{ds}{dt} = \dfrac{dT}{ds}v \end{cases} \tag{10}$$

where, s denotes the independent variable in the spatial S-coordinate and ds is defined as the infinitesimal in this coordinate analogous to dt in the time domain. The process model in

S-coordinate can then be written as:

$$SYS_S : \begin{cases} H' = \dfrac{1}{v} * \dfrac{1}{\tau_H} * \left(\dfrac{4\eta_m \dot{m}_P}{\pi \rho W_0 v} - H \right) \\ T' = \dfrac{1}{v} * \dfrac{1}{\tau_T} * \left(\dfrac{\eta_q q + A_s h_s T_m + A_g h_g T_0}{A_s h_s + A_g h_g} - T \right) \end{cases} \tag{11}$$

where the superscript ($'$) denotes the first-order derivative with respect to s.

Remark 3. It is worth noting that in the above model (in S-coordinate), laser scanning speed is assumed to be non-zero ($v \neq 0$). While this assumption holds for most of the duration of the deposition process, special attention has to be paid to where the velocity approaches zero, such as the two end points of each scan. This is because at these two end points, laser scanning speed is equal or close to 0, while heat conduction is only limited to one direction due to the lack of adjacent material on the other side. This often leads to higher local temperature and hence higher layer build up at the two ends. Special control methods such as the melting pool size based control have been proposed for this [14]. Alternatively, one can consider the controller proposed here to ideally apply away from such end conditions (for example for cladding long parts, where the ends would be discarded by removal processes). In our derivation and discussions of the control schemes below, we exclude similar situations where the velocity approaches zero. Practically, in those situations, the laser power could be turned off by rules excluding start and stop phases.

The control objectives with respect to geometric and thermo-mechanical properties in the final product can be translated into one of depositing layers with desired height profile and melting pool temperature distribution along the deposition track. This can be achieved by adjusting the control inputs (laser power q and scanning speed v) simultaneously.

Furthermore, assume that the coordinate-dependent desired trajectories of layer height and melting pool temperature are $H_d(s)$ and $T_d(s)$, respectively. Define the tracking errors as:

$$e_H = \frac{H - H_d}{H_0}; e_T = \frac{T - T_d}{T_m} \tag{12}$$

in which, H_0 is a constant layer height for normalization and T_m is the melting temperature. The dynamics of the tracking errors can be expressed as:

$$SYS_e : e' = \begin{bmatrix} e'_H \\ e'_T \end{bmatrix} = \begin{bmatrix} F_1(e_H, e_T; u_2) \\ F_2(e_H, e_T; u_1, u_2) \end{bmatrix} = F(e, u) \tag{13}$$

where $e = [e_H, e_T]^T \in X$ and X is the actual state constraint set. The control input vector is denoted as $u = [u_1, u_2]^T = [q/\bar{q}, v/\bar{v}]^T \in U$, which contains the laser power and scanning speed. U is the admissible (normalized) input set and $\bar{q}$, $\bar{v}$ denote the upper bounds of laser power and scanning speed, respectively. It is also possible to include input constraints that consider actuator dynamics (rate of change) in the input set U. The nonlinear functions F_1 and F_2 are short for:

$$F_1 = \frac{1}{H_0} \left[\frac{1}{u_2 \bar{v} \tau_H} \left(\frac{4\eta_m \dot{m}_P}{\pi \rho W_0 \bar{v} u_2} - H_0 e_H - H_d \right) - H'_d \right] \tag{14}$$

$$F_2 = \frac{1}{T_m}\left[\frac{1}{u_2\bar{v}\tau_T}\left(\frac{\eta_q u_1 \bar{q} + A_s h_s T_m + A_g h_g T_0}{A_s h_s + A_g h_g} - e_T T_m - T_d\right) - T_d'\right] \tag{15}$$

With these formulations, the control problem now is defined as one of finding a suitable control input vector u which drives the tracking error vector e to zero. Since the modeling approach involved inevitable reductions and simplifications, the control design should also consider robustness to the uncertainty of the model as well as to other broader disturbances. In the following section, we develop a control scheme that addresses these objectives.

3. Tube-based robust predictive control

The essence of tube-based model predictive control (MPC) method is to incorporate an extra degree of freedom in the MPC framework, via an ancillary control, to improve attenuation of disturbances that arise from uncertainty or process noise [42]. Accordingly, the proposed robust predictive controller design for LAPD processes has the two components detailed below.

3.1. Nominal nonlinear predictive control

We seek to generate the reference input and state trajectories with nonlinear model predictive control. To begin with, the nominal system (with no disturbance/uncertainty) is first defined as:

$$SYS: \ z' = F(z, \gamma) \tag{16}$$

where $z = [e_{\bar{H}}, e_{\bar{T}}]^T = [\frac{\bar{H}-H_d}{H_0}, \frac{\bar{T}-T_d}{T_m}]^T$, $\bar{H}$ and $\bar{T}$ denote the nominal height and temperature, respectively; $\gamma = [\gamma_1, \gamma_2]^T = [q/\bar{q}, v/\bar{v}]^T$ is the nominal input vector. Then, the objective function is defined as follows:

$$J(s_0, z, \gamma) = \int_{s_0}^{s_0+S_p} \mathbb{C}(z(\varsigma), \gamma(\varsigma))d\varsigma + \mathrm{P}\big(z\big(s_0 + S_p\big)\big) \tag{17}$$

where s_0 denotes the current laser position and $S_p = N_p * \Delta s$ is the predictive horizon in the spatial S-coordinate with Δs being the spatial sampling length for the MPC implementation. The first function in the objective is defined as: $\mathbb{C}(z(\varsigma), \gamma(\varsigma)) = z(\varsigma)^T Q z(\varsigma) + \gamma(\varsigma)^T R \gamma(\varsigma)$, where $Q = \begin{bmatrix} q_{11} & 0 \\ 0 & q_{22} \end{bmatrix}, R = \begin{bmatrix} r_{11} & 0 \\ 0 & r_{22} \end{bmatrix}$ are positive-definite matrices with $q_{11}, \ q_{22}, \ r_{11}, \ r_{22} > 0$. The terminal state penalty in the objective function is defined as:

$$\mathrm{P}\big(z\big(s_0 + S_p\big)\big) = \frac{1}{2} z\big(s_0 + S_p\big)^T z\big(s_0 + S_p\big) \tag{18}$$

Then, the nonlinear predictive control for the reference trajectory of the LAPD process is the solution to following optimization problem:

$$min_\gamma \ J(s_0, z, \gamma) \tag{19}$$

$$Subject\ to: \begin{cases} z'(\varsigma) = F(z(\varsigma), \gamma(\varsigma)) \\ z(\varsigma) \in Z \\ \gamma(\varsigma) \in V \\ z(s_0 + S_p) \in \Omega_T \\ \varsigma \in [s_0, s_0 + S_p] \end{cases}$$

where $Z = \alpha_1 X$ and $V = \alpha_2 U$ denote the tightened state and input constraint sets and the two tightening factors are defined as $\alpha_1, \alpha_2 \in (0, 1)$. Ω_T is the terminal state constraint region, which is imposed together with the terminal state penalty in (18) for closed-loop stability [43,44]. From these two stability considerations, a set of inequality constraints on the objective function parameters and the terminal state in MPC are formulated for LAPD processes as follows:

(A) Parameter inequality constraints

$$\begin{cases} q_{11} - \dfrac{1}{\tau_H \bar{v} K_2} \leq 0 \\ q_{22} - \dfrac{1}{\tau_T \bar{v} K_2} + r_{11} {K_1}^2 {K_2}^2 \leq 0 \end{cases} \tag{20}$$

(B) Terminal state inequality constraints

$$\left(\frac{1}{\tau_T T_m \bar{v} K_2} * \frac{A_s h_s T_m + A_g h_g T_0}{A_s h_s + A_g h_g} - \frac{T_d}{\tau_T T_m \bar{v} K_2} - \frac{T'_d}{T_m} \right) * e_T + \left(\frac{4\eta_m \dot{m}_P}{H_0 \tau_H \pi \rho W_0 \bar{v}^2 {K_2}^2} - \frac{H_d}{H_0 \tau_H \bar{v} K_2} - \frac{H'_d}{H_0} \right) * e_H + r_{22} {K_2}^2 \leq 0 \tag{21}$$

where K_1 and K_2 are constant parameters selected for the terminal control. Details about the derivation of the terminal state constraint region are given in the Appendix [21]. Note that these inequality constraints are derived from Lyapunov stability conditions, which are only sufficient but not necessary. Therefore, these two constrains are conservative. Even though it is difficult to explicitly determine the conservativeness of these constraints, constructing different Lyapunov functions could help reduce the conservativeness and improve the controller design for the specific systems.

Remark 4. It is worth noting that with the tightened constraints, only the closed-loop stability for the nominal control can be guaranteed. With the presence of system uncertainties and the resulting additional control efforts (e.g., ancillary control), the tightening strategy can be employed to retain a margin such that satisfaction of actual state and input constraints are guaranteed [45]. For linear systems, these tightened constraint sets can be derived either offline with the concept of robust positive invariant set [28,33], or online with the computation of reachable set [30,31]. However, for complex nonlinear systems such as the LAPD process with coupled nonlinear dynamics, predefining such tightened constraint sets explicitly is very difficult [28,42]. In this paper, two tightening factors (α_1, α_2) are used as an alternative way to simplify the determination of the tightened constraint sets. These two tightening factors could be used as empirical tuning parameters based on the process, such that the actual state and input constraints are satisfied with the presence of process uncertainty. Rigorous determination of the tightened constraints to ensure the closed-loop stability of proposed control still remains as a big challenge.

With the nominal nonlinear predictive control obtained by solving (19) (in a suitably discretized manner), the N-step reference trajectory (z^{N*}, γ^{N*}) can be generated sequentially. In the following, the reference input and state vectors are denoted as: $\gamma^{N*} = [\ \gamma_0{}^* \quad \dots \quad \gamma_{N-1}{}^*\ ]$ and $z^{N*} = [\ z_1{}^* \quad \dots \quad z_N{}^*\ ]$, where $\gamma_i{}^* = \gamma^*(s_0 + i\Delta s)$ and $z_{i+1}{}^* = z^*(s_0 + (i+1)\Delta s),\ i = 0, \dots, N-1$. These will then serve as the central path of the tube to be detailed next.

3.2. Ancillary control

In the framework of tube-based robust control, ancillary control is included to ensure a close tracking of the nominal reference trajectory despite the impact of process uncertainty. For linear systems, this ancillary control is often designed based on local linear state feedback laws *offline* [28,33]. For complex nonlinear systems, Mayne et al. proposed to use a second model predictive controller as the ancillary control for optimal reference trajectory tracking [42]. However, this complicates the control computation by including an extra optimization inside the control loop, especially for fairly complex nonlinear systems. Moreover, quantifying the reachable set (size of the tube) is almost impossible with this design for the present application. In the present paper, we propose an ancillary controller design that is based on the local online linearization along the reference trajectory. This not only simplifies the ancillary control implementation (local linear feedback law instead of nonlinear optimization of MPC), but it also retains the potential of generating tube boundaries for nonlinear systems, similar to the designs for general linear systems.

Given the N-step reference trajectory (z^{N*}, γ^{N*}), the original coupled nonlinear process model in (16) can be linearized along this trajectory as:

$$z' = A^{N*}z + B^{N*}\gamma + \Phi^{N*} + {O_2}^{N*} \tag{22}$$

where the linearized system and input matrices are:

$$A^{N*} = \begin{bmatrix} \dfrac{\partial F_1}{\partial z_1} & \dfrac{\partial F_1}{\partial z_2} \\ \dfrac{\partial F_2}{\partial z_1} & \dfrac{\partial F_2}{\partial z_2} \end{bmatrix}_{|(z^{N*},\gamma^{N*})}, \quad B^{N*} = \begin{bmatrix} 0 & \dfrac{\partial F_1}{\partial \gamma_2} \\ \dfrac{\partial F_2}{\partial \gamma_1} & \dfrac{\partial F_2}{\partial \gamma_2} \end{bmatrix}_{|(z^{N*},\gamma^{N*})}$$

and $\Phi^{N*} = \begin{bmatrix} F_1 - \frac{\partial F_1}{\partial z_1}z_1 - \frac{\partial F_1}{\partial z_2}z_2 - \frac{\partial F_1}{\partial \gamma_2}\gamma_2 \\ F_2 - \frac{\partial F_2}{\partial z_1}z_1 - \frac{\partial F_2}{\partial z_2}z_2 - \frac{\partial F_2}{\partial \gamma_1}\gamma_1 - \frac{\partial F_2}{\partial \gamma_2}\gamma_2 \end{bmatrix}_{|(z^{N*},\gamma^{N*})}$ is the known term. ${O_2}^{N*}$ is the remaining term due to linearization error. After discretization with a suitable sampling length (same as or possibly shorter than Δs), the above Eq. (22) can be rewritten as:

$$z_{k+1} = A_{d,k}z_k + B_{d,k}\gamma_k + \Delta_k \tag{23}$$

in which $A_{d,k}$ and $B_{d,k}$ are the discretized system and input matrices A^{N*} and B^{N*} at step k; Δ_k accounts for the remaining terms in (22), $k = 0, \dots, N-1$. Similarly, the actual system subject to potential disturbance/uncertainty can be expressed as:

$$x_{k+1} = A_{d,k}x_k + B_{d,k}u_k + \Delta_k + w_k \tag{24}$$

where $w_k = [w_{1,k}, w_{2,k}]^T \in W$ is the disturbance vector and is assumed to be additive. W is the admissible set for all possible disturbances.

Defining the mismatch error between the nominal and actual system as $\varepsilon_k = x_k - z_k$, the mismatch dynamics is:

$$\varepsilon_{k+1} = A_{d,k}\varepsilon_k + B_{d,k}(u_k - \gamma_k) + w_k \tag{25}$$

Furthermore, by designing the actual input as:

$$u_k = \gamma_k + u_{ak} \tag{26}$$

and the ancillary control as a local linear state feedback:

$$u_{ak} = K_k \varepsilon_k \tag{27}$$

the mismatch dynamics can be rewritten as:

$$\varepsilon_{k+1} = A_{Kk}\varepsilon_k + w_k \tag{28}$$

where $A_{Kk} = A_{d,k} + B_{d,k}K_k$. To stabilize the mismatch error system via K_k, an infinite-horizon linear quadratic regulator (LQR) is solved with the following objective function:

$$J^{LQR} = \sum_{k=0}^{\infty} \left({\varepsilon_k}^T Q_K \varepsilon_k + {u_{ak}}^T R_K u_{ak} \right) \tag{29}$$

where Q_K and R_K are suitable positive-definite constant matrices to be selected for designing the ancillary control. Furthermore, under the assumption that the initial error is zero, the reachable set at step $k+1$ due to the presence of disturbance w_k can be analyzed as:

$$\mathcal{R}_{k+1} = A_{K\,k}R_k \oplus W \tag{30}$$

in which the operator " $\oplus$ " is the Minkowski sum. This provides a possible way to characterize all the possible deviations of the actual states from their nominal reference values, when uncertainties are present [28,30,33]. Note that the inclusion of feedback gain K_k not only stabilizes the mismatch error system such that a close tracking of the reference trajectory is enforced, but it also attenuates the effects of the disturbance/uncertainty by influencing the size of the reachable set (tube) along the reference trajectory. However, due to the linearization error in ancillary control design and the challenge of explicitly determining the tightening constraint sets to accommodate uncertainties,

The following figure further illustrates the tube-based method.

As shown in Fig. 6, at the initial position of each reference trajectory, the current nominal states are updated with measurements (states) from the actual process. Then, a N-step reference trajectory is generated sequentially with the predictive control formulated in Eq. (19). Within this reference trajectory, local linearization is conducted and the ancillary control is calculated based on real-time sensor measurements. Actual process inputs are then generated and applied successively until the next sensor measurements are available. The computational algorithm is summarized in Table 2.

It is worth mentioning that the computational algorithm in Table 2 is mainly proposed to calculate the ancillary control in addition to the nominal MPC. Given the facts that: (1) the reference trajectory in tube-MPC is generated in the same way as nominal MPC; (2) the reference trajectory is readily available when updating the linearized matrices $(A_{d,k}, B_{d,k})$ and calculating the gain K_k, computational load of the proposed algorithm for tube-MPC is comparable to that of nominal MPC.

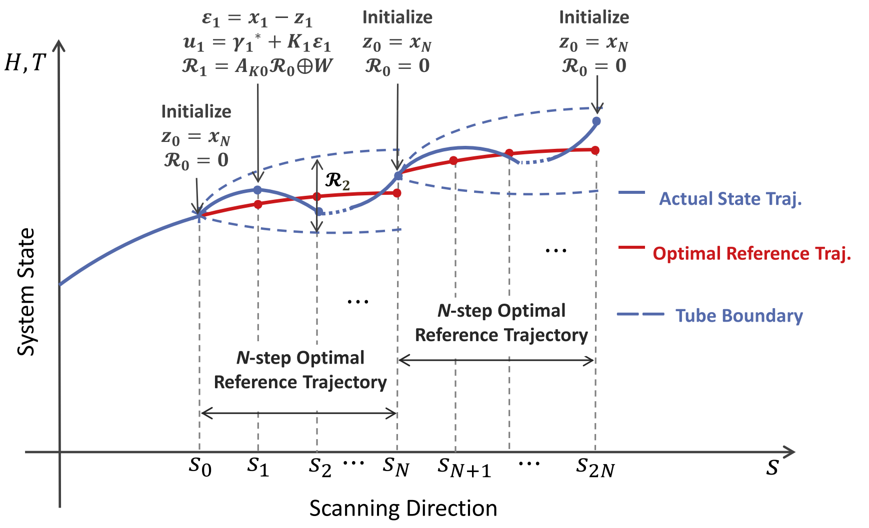

Fig. 6. Illustration of tube-based MPC.

Table 2
Computational algorithm.

Input: State measurements: layer height H, melting pool temperature T.
Output: Process inputs: laser power q, scanning speed v
Step 1: Set $z_0 = x_N$, solve the nominal predictive control problem in (19) sequentially and generate the N-step reference trajectory (z^{N*}, γ^{N*}) with $z^{N*} = [z_1{}^* \quad \ldots \quad z_N{}^*]$ and $\gamma^{N*} = [\gamma_0{}^* \quad \ldots \quad \gamma_{N-1}{}^*]$. Set $k = 0$.
While $k < N$
Step 2: Update the linearized matrices $(A_{d,k}, B_{d,k})$; compute the gain K_k and the actual process input.
Step 3: Apply the input u_k to the actual process.
Step 4: Get the current measurements and update states x_{k+1}; Compute the current reachable set $\mathcal{R}_{k+1}$; Set $k = k + 1$.
End while
Step 5: Go to Step 1

4. Case study

To illustrate the proposed tube-based multivariable predictive control method, laser cladding is considered here as a typical LAPD process. In this process, a thin coating (cladding layer) is deposited on the top surface of a low-carbon steel substrate with a length of 50 mm [10]. An Nd:YAG laser (wavelength of 1.06 μm) with the maximum power of 1.4 kW is used as the heat source and is delivered from the coaxial nozzle head. The powder particles are selected to be the same material as the substrate with an average radius of 50 μm in spherical shape [46]. The scanning speed of the nozzle head is mainly determined by the motion control system and is limited up to 10 mm/s in this application setup. The parameters used in the process model and other process parameters are provided in Table 3.

The major disturbances/uncertainties considered here are assumed to be in the powder catch efficiency η_m and laser absorptivity η_q. With a perturbation of 15% from the nominal values in both of these two process parameters, the deposition height and melting pool

Table 3
Parameters used in simulation.

Parameter	Meaning	Value	Unit
$\boldsymbol{T_m/T_0}$	Melting/ambient temperature	1809/293	[K]
$\boldsymbol{W_0}$	Deposited track-width	2	[mm]
$\boldsymbol{\rho_l}$	Material density	7800	[kg/m^3]
$\boldsymbol{C_l/C_s}$	Liquid/solid heat capacity	804/658	[J/kg/K]
$\boldsymbol{h_s/h_g}$	Heat convection coefficient	1400/24	[W/m^2/K]
$\mathcal{L}$	Latent heat	2.7×10^5	[J/kg]
$\boldsymbol{\dot{m}_p}$	Powder feed rate	8	[g/min]
$\boldsymbol{H_0}$	Layer height constant	1	[mm]
$\boldsymbol{\underline{q}/\bar{q}}$	Laser power bound	400/1400	[W]
$\boldsymbol{\underline{v}/\bar{v}}$	Scanning speed bound	2/10	[mm/s]

temperature deviate from their nominal values with maximum deviations of 0.2 mm and 100 K, respectively. Therefore, the admissible additive disturbance set is assumed to be $W := \{(w_H, w_T)|\ |w_H| \le 0.2$ mm, $|w_T| \le 100$ K$\}$. The nominal nonlinear predictive control is implemented with a sampling length $\Delta s = 0.25$ mm and prediction horizon $N_p = 8$. The control horizon is selected to be the same as the prediction horizon. The length of reference trajectory is selected as $N = 4$. The weighting matrices used in the control objective function of the nominal nonlinear predictive control are: $Q = [1440\ 0; 0\ 510]$, $R = [0.0013\ 0; 0\ 0.0013]$ and the parameters in the terminal control are selected to be: $K_1 = 0.05,\ \ K_2 = 0.6$. These parameters were selected such that the parameter requirements in Eq. (20) are fulfilled with $q_{11} - \frac{1}{\tau_H \bar{v} K_2} = -15.6 < 0$ and $q_{22} - \frac{1}{\tau_T \bar{v} K_2} + r_{11}{K_1}^2{K_2}^2 = -65.1 < 0$. The tightening factors are selected as $\alpha_1 = \alpha_2 = 0.9$. This creates a tightened input constraint set as: $V := \{(\gamma_1, \gamma_2)|\ 0.32 \le \gamma_1 \le 0.96,\ \ 0.24 \le \gamma_2 \le 0.96\}$ for the nominal nonlinear predictive control. As mentioned before, the selection of tightening factor is empirical and mainly depends on the knowledge of system uncertainty. With a low process uncertainty, high tightening factor (less tightening in nominal MPC) is desirable to optimize the reference trajectory, since the mismatch between the actual system and the model is expected to be small. This leads to less control effort from the ancillary control. By contrast, with a high process uncertainty, low tightening factor is preferable in order to reserve a margin for the ancillary control. An additional input constraint that considers the actuator dynamics is also imposed as: $\Delta V := \{(\Delta\gamma_1, \Delta\gamma_2)|\ |\Delta\gamma_1| \le 0.21,\ \ |\Delta\gamma_2| \le 0.20\}$, in which $\Delta\gamma_{1,2}$ denotes the variation between two successive input sequences in the MPC formulation. No particular state constraints other than the process dynamics are imposed in this case. For the ancillary control design, the LQR weighting matrices are selected as $Q_K = [100\ 0; 0\ 10],\ \ R_K = [1\ 0; 0\ 0.1]$. These parameters are kept the same in the following case studies.

To demonstrate the simultaneous control of layer height and melting pool temperature, desired profiles of these two properties are first pre-designed as shown in Fig. 7. The desired deposition height profile is assumed to be sinusoidal. This is often met in manufacturing complex parts where deposition of a continuously variable geometry is required. Meanwhile, the desired temperature profile has constant levels at different sections (with proper ramp rates) to meet specific thermo-mechanical properties along the track for part quality [47]. With a disturbance of 10% included in both the powder catch efficiency and the laser absorptivity, the control performance of the proposed method is shown in Figs. 7–9.

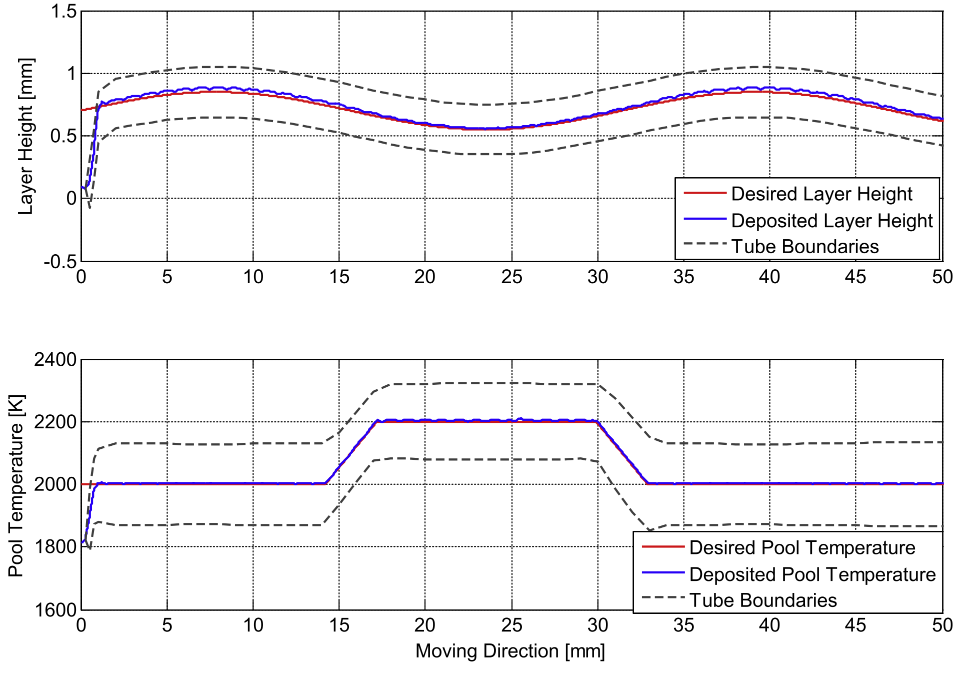

Fig. 7. Layer height and pool temperature with tube-based MPC, the tube boundary (dashed line) is generated based on the admissible additive disturbance set $W := \{(w_H, w_T)|\ |w_H| \le 0.2$ mm, $|w_T| \le 100$ K$\}$.

Fig. 7 shows the deposition layer height and melting pool temperature under the proposed control. The tube boundaries consist of all the reachable sets at each sampling location and quantify the range of all the possible state trajectories with the presence of potential disturbances (uncertainties in η_m and η_q). As we can see, the actual layer height and pool temperature follow their desired values closely within their tube boundaries. The laser power input applied by the nominal/reference nonlinear MPC as well as the ancillary control components in the tube-based MPC are shown in Fig. 8 and the scanning speed components are shown in Fig. 9.

With the tube-based MPC, the final applied laser power is manipulated around its nominal reference value generated by the nominal nonlinear predictive control. The ancillary control of laser power, which contributes to the deviation from its nominal reference value, is only involved locally to compensate for disturbances in the actual process. Similarly, the scanning speed components applied by the tube-based MPC are illustrated in Fig. 9.

Note that with the potential (uncertain) increase of powder catch efficiency and laser absorptivity in the actual process, the ancillary control tends to accelerate the scanning speed from its nominal reference value. This helps to diminish the effects of increased local heat transfer and material deposition, thus maintaining the same deposition height and pool temperature as in the nominal case. Furthermore, the actual control inputs are bounded and no significant actuator saturation is found with the selected constrained tightening factor in the nominal MPC.

To further demonstrate the efficacy of the tube-based method, comparisons with the control performance of non-tube MPC (where the ancillary control *is not activated*) are illustrated in

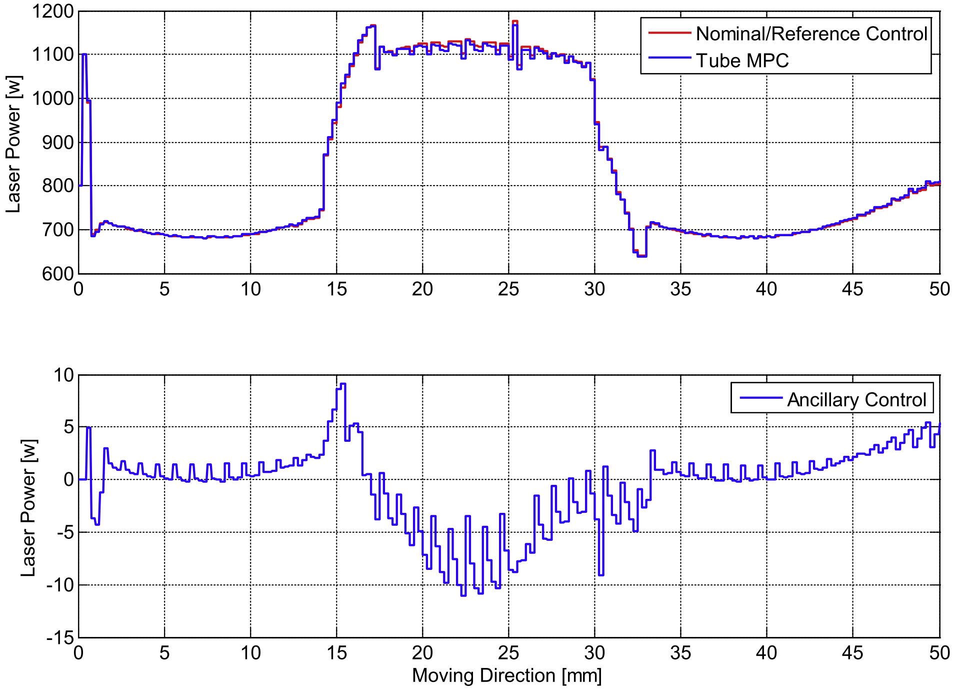

Fig. 8. Laser power applied by the tube-based MPC. The ancillary control in the second plot is the difference between the actual and nominal reference input in the first plot.

Figs. 10 and 11. It is important to note that the sampling length and the prediction/control horizons are setup the same for both non-tube MPC and tube MPC. This is based on the assumptions that computational power/resources are similarly available to both controllers. Moreover, the nonlinear optimization inherent in nonlinear MPC is generally more computational intensive than the local linear state feedback control embedded in the ancillary control.

As we can see from Fig. 10, noticeable deviations of both the deposited layer height and pool temperature from their desired values can be seen with the non-tube MPC. This is mainly due to the lack of the ancillary control for local feedback and disturbance compensation. This can be further observed from the error comparisons in Fig. 11.

Compared to the maximum height error with the proposed method at around 0.03 mm, the non-tube predictive control generates a maximum height error around 0.08 mm for deposition of this single layer. This difference becomes much more pronounced (superimposes) when manufacturing thick components with multiple-layer depositions. Moreover, an improvement on the surface finish quality with respect to the roughness can also be observed with the proposed method. This stems from the fact that within each optimal reference trajectory (1 mm length given $N = 4$ in Table 2), the potential disturbances due to the mismatch in powder catch efficiency and the laser absorptivity are compensated with the ancillary control. This helps to improve the dimensional accuracy of finished products, which is currently a major concern with most additive manufacturing processes such as LAPD. As a comparison, the no-tube MPC only tracks the optimal reference trajectory without any consideration on disturbances. This leads to a larger propagated error over the reference trajectory and hence a

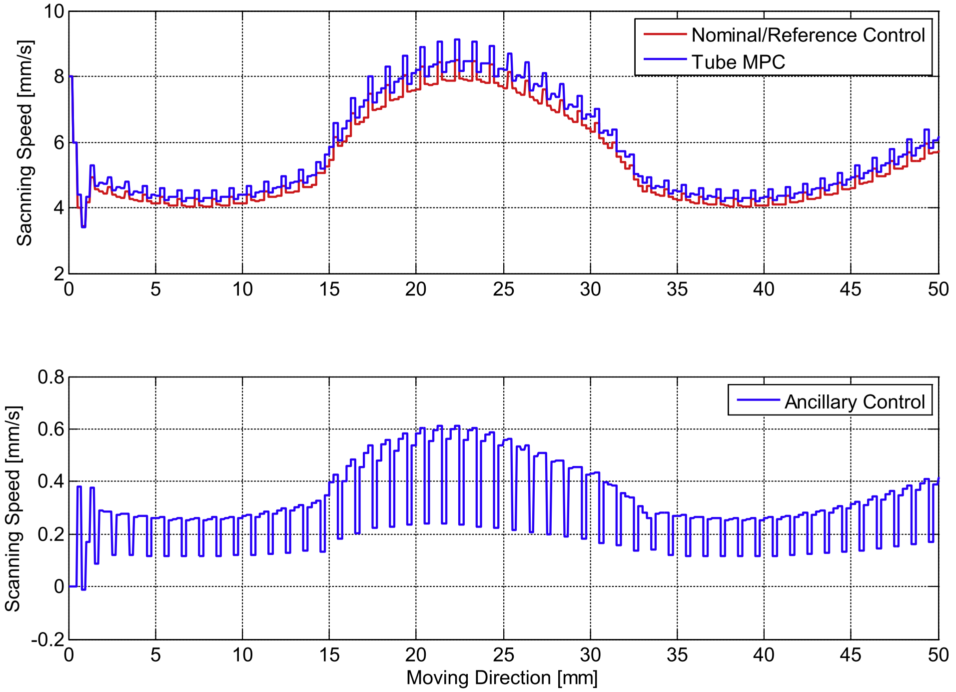

Fig. 9. Scanning speed applied with tube-based MPC.

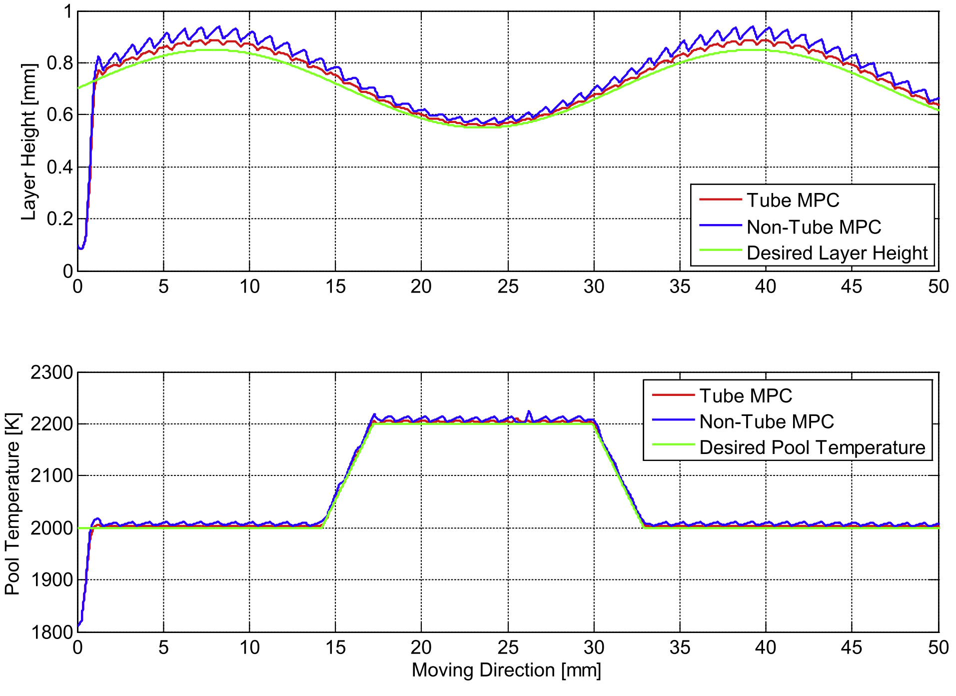

Fig. 10. Comparison of layer height and pool temperature between tube MPC and non-tube MPC.

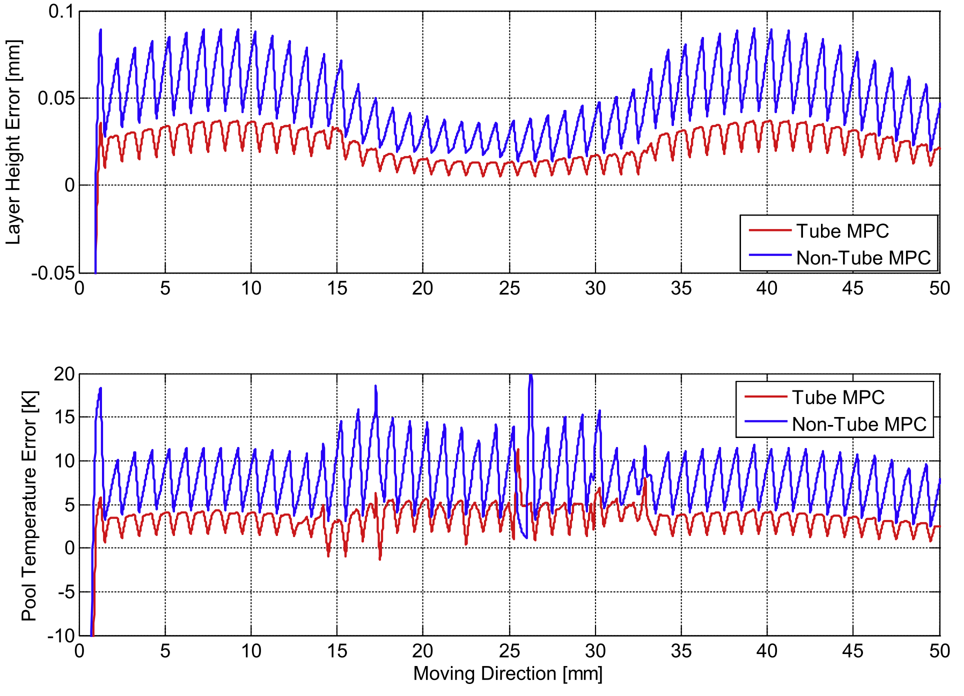

Fig. 11. Comparison of layer height error and pool temperature error between tube MPC and non-tube MPC.

much rougher surface finish as a result. Similar improvement on the control of melting pool temperature can be found, where the average temperature error is less than 5 K, compared with that around 10 K in the non-tube case. This further supports the claims in the proposed control method.

With the aim of exploring the potential of this tube-based predictive control method, a comparison case study is provided that considers the design of the ancillary control. By designing different weighting matrices in the LQR formulation, different local feedback gains can be generated for the ancillary control, thus affecting the performance of the proposed control method. Here, we consider two different ancillary controls with the weighting matrices as: Ancillary control 1: $Q_K = \begin{bmatrix} 100 & 0 \\ 0 & 10 \end{bmatrix}, R_K = \begin{bmatrix} 1 & 0 \\ 0 & 0.1 \end{bmatrix}$; Ancillary control 2: $Q_K = \begin{bmatrix} 1 & 0 \\ 0 & 1 \end{bmatrix}, R_K = \begin{bmatrix} 1 & 0 \\ 0 & 1 \end{bmatrix}$. The performance comparisons are demonstrated in Figs. 12 and 13.

As shown in Fig. 12, with a relatively larger weighting matrix (Q_K) for the states, minimizing the mismatch errors between the reference and the actual process states is prioritized, leading to a more aggressive ancillary control for reference tracking. This is further demonstrated in Fig. 13, where both the tracking errors of layer height and pool temperature are improved. However, it is worth noting that further improvement is not guaranteed by designing the weighting matrices as the actual system is nonlinear; it is only locally linearized for the purposed of designing the ancillary control. This could also be limited by factors such as

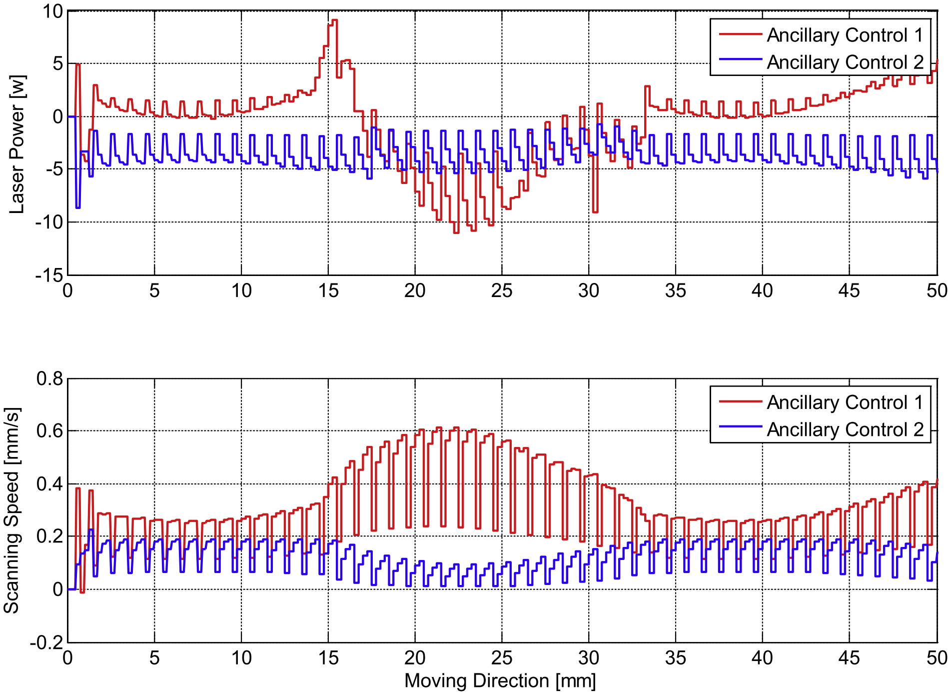

Fig. 12. Comparison of different ancillary controls.

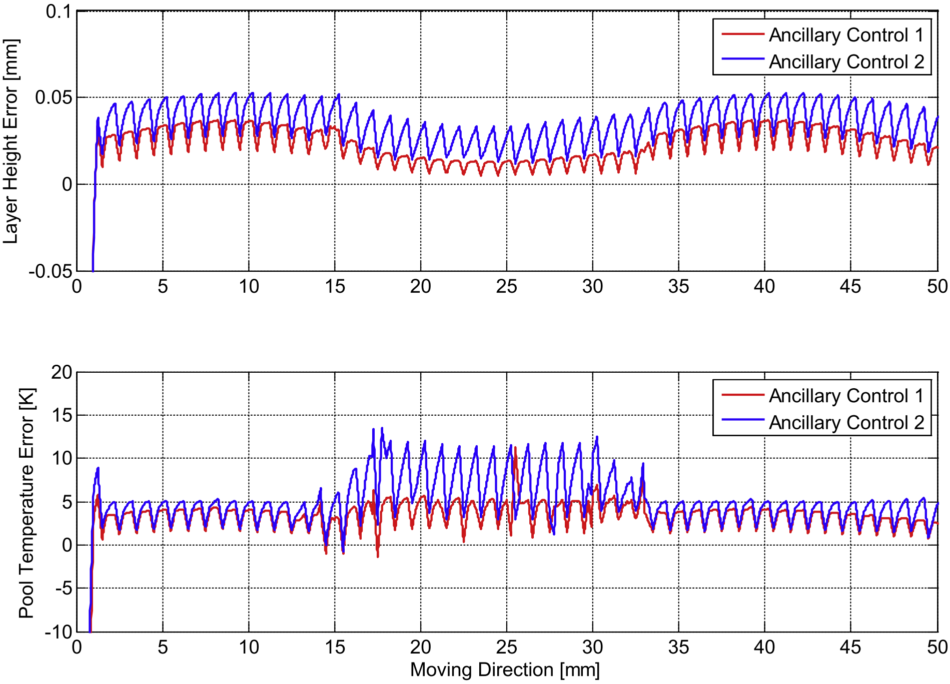

Fig. 13. Errors of layer height and melting pool temperature with different ancillary controls.

the length of reference trajectory as well as the constraints of the actuators (motion system and laser source).

5. Conclusion

This paper outlined a tube-based multivariable predictive control method for a class of laser-aided powder deposition (LAPD) processes. It employs a novel control-oriented *MIMO* model that attempts to bridge the gap between the complexity of the multi-physics processes and the needs for model-based control design. The tube-based robust predictive control design combines the nominal/optimal reference trajectories generated with nonlinear MPC and an ancillary control design based on local linearization. Case studies on the laser cladding process are included to demonstrate the effectiveness of the proposed control design in the presence of potential parameter uncertainties (powder catch efficiency and laser absorptivity). The tunability of the ancillary control design is also discussed.

Finally, we remark that the control system design outlined in this paper is a first attempt to design a predictive control scheme for complex LAPD processes from a *MIMO* design perspective along with the consideration of robustness to uncertainties/disturbances. However, to fully explore control opportunities to optimize product quality, further development of control-oriented high-fidelity mathematical models that consider a wider range of operating conditions (e.g., powder feed rate, nozzle standoff distance/orientation.), are still needed. Furthermore, a PDE-based online control system design that is capable of dealing with strong spatial distribution issues in LAPD processes, such as thermal gradients and dilution/penetration depth, is largely an open area.

Acknowledgment

The authors acknowledge the financial support received for this research, in part, from the US National Science Foundation under NSF Grant No. CMMI-1055254 and the U.S. Department of Energy (DOE) Graduate Automotive Technology Education Program under grant No. DE-EE0005571.

Appendix. Derivation of the nominal stability condition

In this appendix, the closed-loop stability of LAPD processes with the proposed nonlinear MPC scheme is analyzed based on the following theorem re-stated from [44,48].

Theorem 1 [44,48]. *Suppose the reference control signals are bounded and the optimization problem is feasible at $\varsigma = s_0$. Under the model predictive control algorithm described previously for the system (SYS_e), it's origin is asymptotically stable if a terminal state controller $u_T(s_0 + S_p)$ exists such that the following condition is satisfied:*

$$P'\big(e\big(s_0 + S_p\big)\big) + \mathbb{C}\big(e\big(s_0 + S_p\big), u_T\big(s_0 + S_p\big)\big) \leq 0 \tag{A.1}$$

for any state $e(s_0 + S_p)$ belonging to the terminal region Ω_T.

In the following, we analyze the terminal state in LAPD process. The coordinate variable $s_0 + S_p$ is omitted for brevity. According to Theorem 1, we have:

$$P'(e) + \mathbb{C}(e, u) = e^T e' + e^T Qe + u^T Ru$$

$$
\begin{aligned}
&= [e_H \quad e_T]\begin{bmatrix} F_1 \\ F_2 \end{bmatrix} + q_{11}{e_H}^2 + q_{22}{e_T}^2 + r_{11}{u_1}^2 + r_{22}{u_2}^2 \\
&= \frac{1}{H_0\bar{v}\tau_H} * \frac{4\eta_m \dot{m}_P}{\pi\rho W_0\bar{v}} * \frac{e_H}{{u_2}^2} - \frac{1}{\tau_H\bar{v}u_2} * {e_H}^2 - \frac{1}{\tau_T\bar{v}u_2} * {e_T}^2 \\
&\quad - \left(\frac{H_d}{H_0\tau_H\bar{v}u_2} + \frac{H_d'}{H_0}\right) * e_H - \left(\frac{T_d}{\tau_T T_m\bar{v}u_2} + \frac{T_d'}{T_m}\right) * e_T + \frac{1}{\tau_T T_m\bar{v}} \\
&\quad * \frac{\eta_q u_1\bar{q} + A_s h_s T_m + A_g h_g T_0}{A_s h_s + A_g h_g} * \frac{e_T}{u_2} + q_{11}{e_H}^2 + q_{22}{e_T}^2 + r_{11}{u_1}^2 + r_{22}{u_2}^2
\end{aligned}
\tag{A.2}
$$

Define the terminal control as:

$$
u_T = \begin{bmatrix} u_1 \\ u_2 \end{bmatrix} = \begin{bmatrix} -K_1 u_2 e_T \\ K_2 \end{bmatrix} \tag{A.3}
$$

where $K_1,\ K_2$ are positive constants. Then, rewrite Eq. (A.2) as:

$$
\begin{aligned}
P'(e) + \mathbb{C}(e,u) &= \left(\frac{1}{H_0\bar{v}\tau_H} * \frac{4\eta_m\dot{m}_P}{\pi\rho W_0\bar{v}{K_2}^2} - \frac{H_d}{H_0\tau_H\bar{v}K_2} - \frac{H_d'}{H_0}\right) * e_H + \left(\frac{1}{\tau_T T_m\bar{v}K_2} * \frac{A_s h_s T_m + A_g h_g T_0}{A_s h_s + A_g h_g} - \frac{T_d}{\tau_T T_m\bar{v}K_2} - \frac{T_d'}{T_m}\right) \\
&\quad * e_T + \left(q_{22} - \frac{1}{\tau_T\bar{v}K_2} - \frac{1}{\tau_T T_m\bar{v}} * \frac{\eta_q K_1\bar{q}}{A_s h_s + A_g h_g} + r_{11}{K_1}^2{K_2}^2\right) * {e_T}^2 + \left(q_{11} - \frac{1}{\tau_H\bar{v}K_2}\right) * {e_H}^2 + r_{22}{K_2}^2
\end{aligned}
\tag{A.4}
$$

According to Theorem 1, the following design parameter constraints and terminal state constraint have to be satisfied:

Requirements of parameters:

$$
\begin{cases} q_{11} - \dfrac{1}{\tau_H\bar{v}K_2} \le 0 \\ q_{22} - \dfrac{1}{\tau_T\bar{v}K_2} + r_{11}{K_1}^2{K_2}^2 \le 0 \end{cases} \tag{A.5}
$$

Terminal state inequality constraint:

$$
\left(\frac{1}{\tau_T T_m\bar{v}K_2} * \frac{A_s h_s T_m + A_g h_g T_0}{A_s h_s + A_g h_g} - \frac{T_d}{\tau_T T_m\bar{v}K_2} - \frac{T_d'}{T_m}\right) * e_T + \left(\frac{4\eta_m\dot{m}_P}{H_0\tau_H\pi\rho W_0\bar{v}^2{K_2}^2} - \frac{H_d}{H_0\tau_H\bar{v}K_2} - \frac{H_d'}{H_0}\right) * e_H + r_{22}{K_2}^2 \le 0 \tag{A.6}
$$

Note that by imposing the second inequality in the parameter requirements, the following inequality is implied:

$$
q_{22} - \frac{1}{\tau_T\bar{v}K_2} - \frac{1}{\tau_T T_m\bar{v}} * \frac{\eta_q K_1\bar{q}}{A_s h_s + A_g h_g} + r_{11}{K_1}^2{K_2}^2 \le 0 \tag{A.7}
$$

The design parameters in the terminal control Eq. (A.3) and the objective function Eq. (17) should be selected to fulfill the parameter requirements Eq. (A.5). Then, by adding the terminal state inequality Eq. (A.6) into the MPC constraints, the inequality condition Eq. (A.1) is satisfied in Theorem 1.

References

[1] J. Laeng, J. Stewart, F.W. Liou, Laser metal forming processes for rapid prototyping – a review, Int. J. Prod. Res. 38 (2000) 3973–3996.

[2] I. Gibson, D.W. Rosen, B. Stucker, Additive Manufacturing Technologies, Springer, 2010.
[3] G. Tapia, A. Elwany, A review on process monitoring and control in metal-based additive manufacturing, J. Manuf. Sci. Eng. 136 (2014) 060801.
[4] C. Beyer, Strategic implications of current trends in additive manufacturing, J. Manuf. Sci. Eng. 136 (2014) 064701.
[5] M.R. Boddu, V.P. Thayalan, R.G. Landers, Modeling for the control of the laser aided manufacturing process (LAMP), in: Proceedings of the Fourteenth Annual Solid Freeform Fabrication Symposium, 2003, pp. 4–6.
[6] A. Fathi, A. Khajepour, E. Toyserkani, M. Durali, Clad height control in laser solid freeform fabrication using a feedforward PID controller, Int. J. Adv. Manuf. Technol. 35 (2007) 280–292.
[7] L. Song, J. Mazumder, Feedback control of melt pool temperature during laser cladding process, IEEE Trans. Control Syst. Technol. 19 (2011) 1349–1356.
[8] S. Morville, M. Carin, P. Peyre, M. Gharbi, D. Carron, P. Le Masson, et al., 2D longitudinal modeling of heat transfer and fluid flow during multilayered direct laser metal deposition process, J. Laser Appl. 24 (2012) 032008.
[9] S. Wen, Y.C. Shin, Modeling of transport phenomena during the coaxial laser direct deposition process, J. Appl. Phys. 108 (2010) 044908.
[10] H. Qi, J. Mazumder, H. Ki, Numerical simulation of heat transfer and fluid flow in coaxial laser cladding process for direct metal deposition, J. Appl. Phys. 100 (2006) 024903.
[11] L. Han, F. Liou, Numerical investigation of the influence of laser beam mode on melt pool, Int. J. Heat Mass Transf. 47 (2004) 4385–4402.
[12] J. Hofman, B. Pathiraj, J. van Dijk, D. de Lange, J. Meijer, A camera based feedback control strategy for the laser cladding process, J. Mater. Process. Technol. (2012).
[13] D. Salehi, M. Brandt, Melt pool temperature control using LabVIEW in Nd: YAG laser blown powder cladding process, int. J. Adv. Manuf. Technol. 29 (2006) 273–278.
[14] D. Hu, R. Kovacevic, Sensing, modeling and control for laser-based additive manufacturing, Int. J. Mach. Tools Manuf. 43 (2003) 51–60.
[15] E. Toyserkani, A. Khajepour, A mechatronics approach to laser powder deposition process, Mechatronics 16 (2006) 631–641.
[16] C. Doumanidis, Y.-M. Kwak, Geometry modeling and control by infrared and laser sensing in thermal manufacturing with material deposition, J. Manuf. Sci. Eng. 123 (2001) 45–52.
[17] A. Fathi, A. Khajepour, M. Durali, E. Toyserkani, Geometry control of the deposited layer in a nonplanar laser cladding process using a variable structure controller, J. Manuf. Sci. Eng. 130 (2008) 031003.
[18] L. Tang, R.G. Landers, Layer-to-layer height control for laser metal deposition process, J. Manuf. Sci. Eng. 133 (2011) 021009.
[19] L. Song, V. Bagavath-Singh, B. Dutta, J. Mazumder, Control of melt pool temperature and deposition height during direct metal deposition process, Int. J. Adv. Manuf. Technol. 58 (2012) 247–256.
[20] D.Q. Mayne, J.B. Rawlings, C.V. Rao, P.O. Scokaert, Constrained model predictive control: stability and optimality, Automatica 36 (2000) 789–814.
[21] X. Cao, B. Ayalew, Multivariable predictive control of laser-aided powder deposition processes, in: Proceedings of the American Control Conference, 2015, pp. 3625–3630.
[22] S. Yu, M. Reble, H. Chen, F. Allgöwer, Inherent robustness properties of quasi-infinite horizon nonlinear model predictive control, Automatica 50 (9) (2014) 2269–2280.
[23] L. Magni, H. Nijmeijer, A. Van Der Schaft, A receding-horizon approach to the nonlinear H∞ control problem, Automatica 37 (2001) 429–435.
[24] L. Magni, G. De Nicolao, R. Scattolini, F. Allgöwer, Robust model predictive control for nonlinear discrete-time systems, Int. J. Robust Nonlinear Control 13 (2003) 229–246.
[25] M.R. James, J.S. Baras, Robust H∞ output feedback control for nonlinear systems, IEEE Trans. Autom. Control 40 (1995) 1007–1017.
[26] A. Richards, J. How, Robust stable model predictive control with constraint tightening, in: Proceedings of the American Control Conference, 2006, p. 6. pp.
[27] L. Chisci, J.A. Rossiter, G. Zappa, Systems with persistent disturbances: predictive control with restricted constraints, Automatica 37 (2001) 1019–1028.
[28] J.B. Rawlings, D.Q. Mayne, Model Predictive control: Theory and Design, Nob Hill Pub., 2009.
[29] D.Q. Mayne, M.M. Seron, S. Raković, Robust model predictive control of constrained linear systems with bounded disturbances, Automatica 41 (2005) 219–224.

[30] R. Gonzalez, M. Fiacchini, T. Alamo, J. Guzman, F. Rodriguez, Online robust tube-based MPC for time-varying systems: a practical approach, Int. J. Control 84 (2011) 1157–1170.
[31] R. González, M. Fiacchini, J.L. Guzmán, T. Álamo, F. Rodríguez, Robust tube-based predictive control for mobile robots in off-road conditions, Rob. Autom. Syst. 59 (2011) 711–726.
[32] Y. Gao, A. Gray, A. Carvalho, H.E. Tseng, F. Borrelli, Robust nonlinear predictive control for semiautonomous ground vehicles, in: Proceedings of the American Control Conference (ACC, 2014, pp. 4913–4918.
[33] Y. Gao, A. Gray, H.E. Tseng, F. Borrelli, A tube-based robust nonlinear predictive control approach to semiautonomous ground vehicles, Veh. Syst. Dyn. 52 (6) (2014) 802–823.
[34] X. Cao, B. Ayalew, Control-oriented MIMO modeling of laser-aided powder deposition processes, in: Proceedings of the American Control Conference, 2015, pp. 3637–3642.
[35] J.T. Hofman, Development of an Observation and Control System For Industrial Laser Cladding, University of Twente, 2009.
[36] I. Medina and J. Ramses, "Development and application of a CFD model of laser metal deposition," 2013.
[37] A.J. Pinkerton, L. Li, Modelling the geometry of a moving laser melt pool and deposition track via energy and mass balances, J. Phys. D Appl. Phys. 37 (2004) 1885.
[38] A. Fathi, E. Toyserkani, A. Khajepour, M. Durali, Prediction of melt pool depth and dilution in laser powder deposition, J. Phys. D Appl. Phys. 39 (2006) 2613.
[39] H. Gedda, Laser Cladding: An Experimental and Theoretical Investigation Ph. D. thesis, Luleå University of Technology, Luleå, 2004.
[40] E. Toyserkani, A. Khajepour, S.F. Corbin, Laser Cladding, CRC press, 2004.
[41] N. Al-Khalidy, Application of optimization methods for solving inverse phase-change problems, Numer. Heat Transf. 31 (1997) 477–497.
[42] D. Mayne, E. Kerrigan, E. Van Wyk, P. Falugi, Tube-based robust nonlinear model predictive control, Int. J. Robust Nonlinear Control 21 (2011) 1341–1353.
[43] H. Michalska, D.Q. Mayne, Robust receding horizon control of constrained nonlinear systems, IEEE Trans. Autom. Control 38 (1993) 1623–1633.
[44] W.-H. Chen, D.J. Ballance, J. O'Reilly, Model predictive control of nonlinear systems: computational burden and stability, in: Proceedings of the IEE Control Theory and Applications, 2000, pp. 387–394.
[45] S. Yu, C. Bohm, H. Chen, F. Allgower, Robust model predictive control with disturbance invariant sets, in: Proceedings of the American Control Conference (ACC), 2010, pp. 6262–6267.
[46] L. Han, K. Phatak, F. Liou, Modeling of laser cladding with powder injection, Metall. Mater. Trans. B 35 (2004) 1139–1150.
[47] N. Hopkinson, R. Hague, P. Dickens, Rapid Manufacturing: An Industrial Revolution for the Digital Age, John Wiley & Sons, 2006.
[48] D. Gu, H. Hu, Receding horizon tracking control of wheeled mobile robots, IEEE Trans. Control Syst. Technol. 14 (2006) 743–749.